Developmental Cell, Volume *27*

Supplemental Information

The Plasma Membrane Flattens Out to Fuel Cell-Surface Growth during *Drosophila* Cellularization

Lauren Figard, Heng Xu, Hernan G. Garcia, Ido Golding, and Anna Marie Sokac

Inventory of Supplementary Materials:

Figure S1: Related to Figure 1, this figure shows high magnification scanning electron micrographs of microvilli, and illustrates the models used for the minimum/maximum calculations in Figure 1.

Figure S2: Related to Figure 2, this figure shows confocal images of Venus-PH-PLCδ labeling the microvilli, with additional controls to support conclusions from Figure 2.

Figure S3: Related to Figures 2 and 3, this figure shows the distribution of instantaneous velocities for furrow ingression, and the normalized fluorescence versus furrow length plots for the additional microvillar membrane markers shown in Figure S2.

Figure S4: Related to Figures 3 and 4, this figure shows confocal images of microvillar depletion in abl^{RNAi} embryos, and redistribution of 1x-WGA^{AX594} into the furrows, independent of endocytosis.

Table S1: Related to Figure 1, this table provides the dimensions of microvilli used in the minimum/maximum calculations, and compares the dimensions to published values.

Table S2: Related to Figures 2, 3, 4, and S4, this table provides furrow ingression velocities measured for different imaging methods.

Movie S1: Related to Figure 2, this is an example of a movie from which furrow ingression kinetics were measured.

Movie S2: Related to Figure 2, this movie is an example of the output from our MATLAB code, tracking furrow position with time to generate the ingression trajectories in Figure 2F.

Supplemental Experimental Procedures

Supplemental References

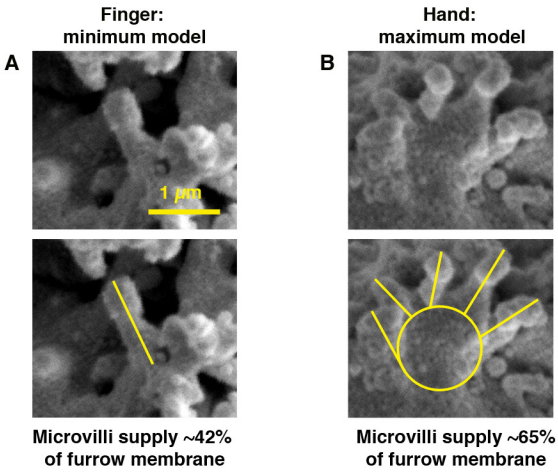

Figure S1. SEM images of representative microvilli from embryos at early cellularization; related to Figure 1. (A) Panels showing a microvillus with overlay to illustrate the finger model. For the minimum calculation, the microvillus was treated as a cylinder (line). **(B)** Panels showing a microvillar complex with overlay to illustrate the hand model. For the maximum calculation, the complex was treated as a squat cylindrical base (circle) topped with 5 cylindrical microvilli (lines). Percent furrow membrane (mean) provided by each model is shown below its respective images.

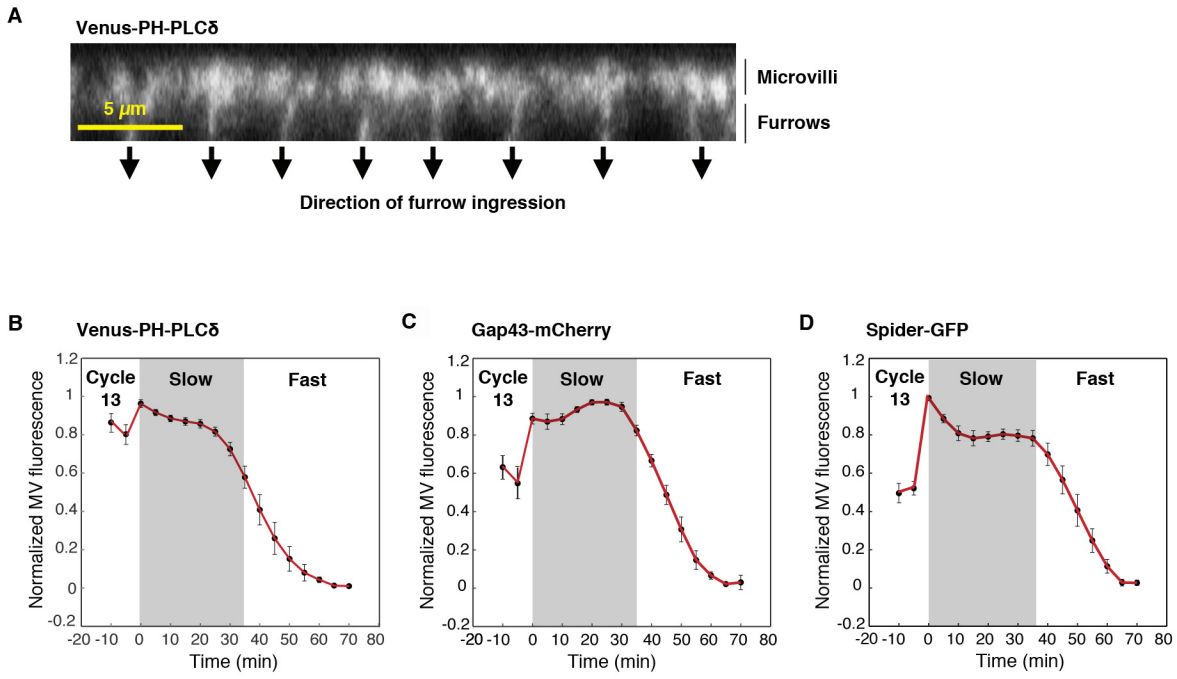

Figure S2. Microvillar membrane is depleted with biphasic kinetics; related to Figure 2. **(A)** Projected cross-section showing Venus-PH-PLCδ localizes to microvilli and furrows. Furrows and direction of ingression indicated by arrows. **(B)** Quantification of average normalized apical fluorescence intensity versus time for Venus-PH-PLCδ (n=8 embryos; mean ± SE), **(C)** Gap43-mCherry (n=7 embryos; mean ± SE), and **(D)** Spider-GFP (n=7 embryos; mean ± SE). Slow depletion phase is shaded. Cycle 13 data included here to show that our method can measure increases as well as decreases in fluorescence. Solid line is a spline through the data points.

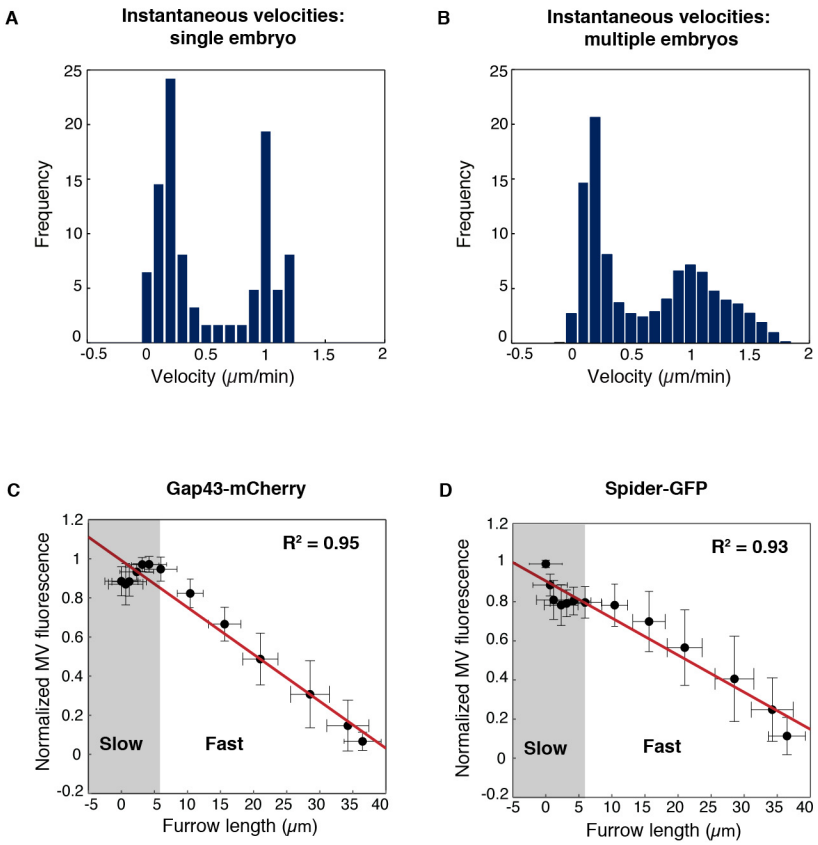

Figure S3. Furrow ingression is biphasic, and linearly related to microvillar depletion; related to Figure 2. Quantification showing frequency of instantaneous furrow ingression velocities from **(A)** a single embryo (n=30 trajectories from 1 embryo), and **(B)** all embryos (n=353 trajectories from 12 embryos). Frequency is the percent trajectories with the indicated velocity. Velocities cluster into a slow and a fast phase during cellularization. **(C)** Quantification of average normalized fluorescence intensity of microvillar membrane versus furrow length for Gap43-mCherry (n=7 embryos; mean $\pm$ SD), and **(D)** Spider-GFP (n=7 embryos; mean $\pm$ SD). Line is a linear least square fit.

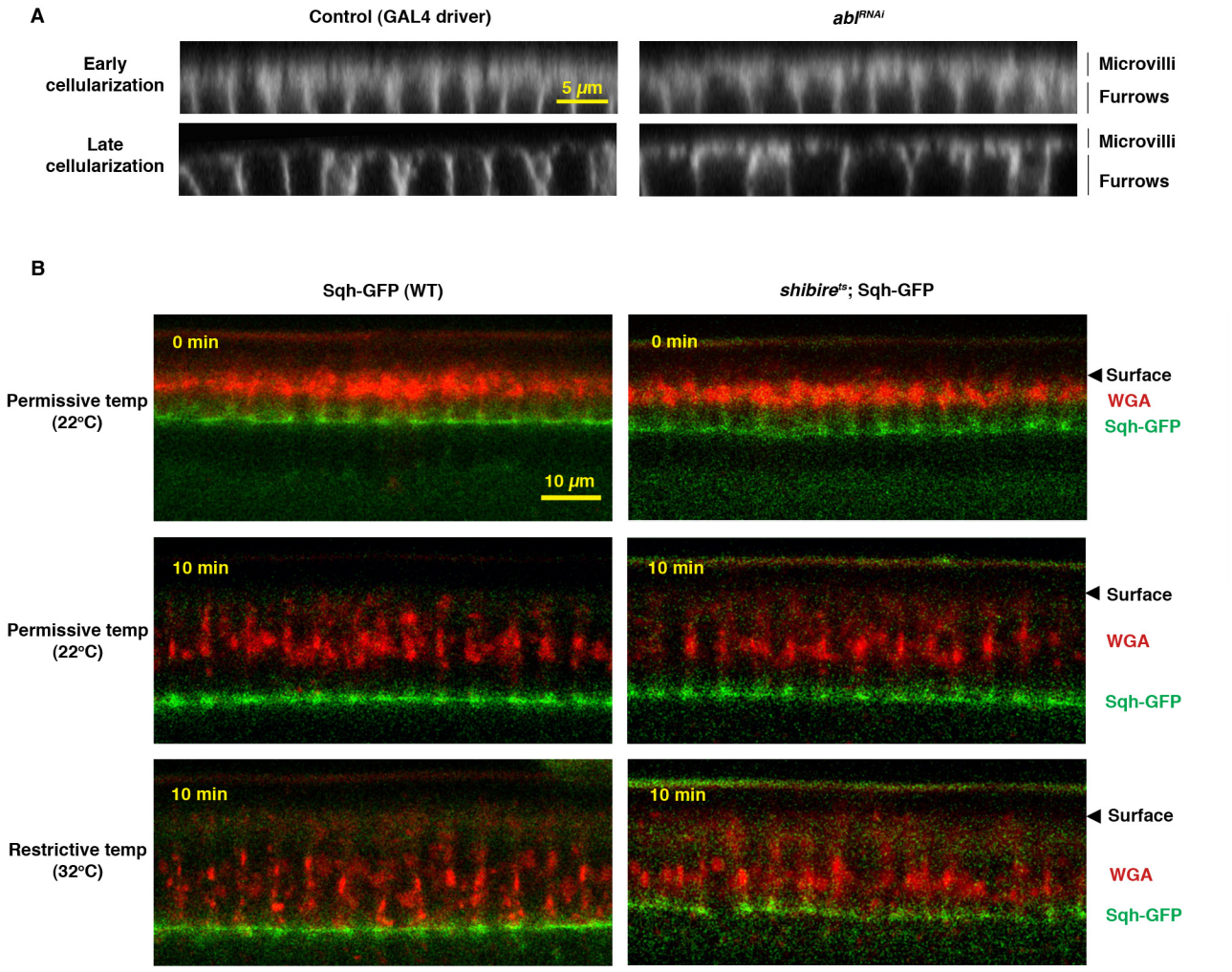

Figure S4. Microvillar membrane moves into ingressing furrows, independent of endocytosis; related to Figures 3 and 4. (A) Projected cross-section showing more microvilli (phalloidin^{AX546} stained F-actin) are maintained at late cellularization in *abl*^{RNAi} embryos than in controls. **(B)** Cross-sections in Sqh-GFP (WT; wild-type) and *shibire*^{ts}; Sqh-GFP embryos showing microvillar membrane (1x-WGA^{AX594}; red) on the apical surface at 0 minutes post-injection and in the furrows at 10 minutes after injection at either permissive (22°C) or restrictive (32°C) temperature. Sqh-GFP (green) marks furrow tips.

Table S1: Measured and published microvilli (MV) dimensions

	Cellularizing embryos	Mouse cultured cells	Chicken intestinal cells
MV diameter (nm)	585 ± 69	100	100
MV length (nm)	2098 ± 581	400	1000-2000

Table S1. Microvillar dimensions from SEM surface images of embryos; related to Figure 1. Measurements are from early cellularization (n=5 microvilli; mean ± SD). Published values for microvilli from mouse cultured cells (Knutton et al., 1975) and chicken intestinal cells (Mooseker and Tilney, 1975) are included for comparison.

Table S2: Furrow ingression velocities for different imaging methods

	Slow phase velocity (μm/min)	Fast phase velocity (μm/min)
Sqh-GFP	0.2 ± 0.01	1.3 ± 0.04
OreR	0.2 ± 0.02	1.2 ± 0.10
Sqh-GFP; RNAi control	0.2 ± 0.01	1.3 ± 0.02
Sqh-GFP; WGA-injected	N/A	1.1 ± 0.04
***shibire*^{ts}; Sqh-GFP**	N/A	0.8 ± 0.11

Table S2. Furrow ingression velocities for different methods of embryo imaging; related to Figures 2, 3, 4 and S4. For Sqh-GFP, ingression was imaged and analyzed with the automated MATLAB code (n=353 trajectories from 12 embryos; mean ± SE). For OreR, ingression was imaged by DIC and analyzed manually (n=4 furrows from 2 embryos; mean ± SE). For Sqh-GFP RNAi buffer-injected control, ingression was imaged and analyzed with the automated MATLAB code (n=259 trajectories from 10 embryos; mean ± SE). For Sqh-GFP; 1x-WGA^{AX594} injected, ingression was imaged and analyzed manually (n=6 furrows from 3 embryos; mean ± SE). N/A indicates that measurement is not available because 1x-WGA^{AX594} injection was done during slow phase. For *shibire*^{ts}; Sqh-GFP, ingression was imaged and analyzed manually (n=4 furrows from 2 embryos; mean ± SE). N/A indicates that measurement is not available because heat shock of *shibire*^{ts} during slow phase stalls ingression (Pelissier et al., 2003).

Movie S1. Time-lapse movie showing the moving front of Sqh-GFP during furrow ingression; related to Figure 2. Time shown is hours:minutes. Regression of pseudocleavage furrows in mitotic cycle 13 precedes cellularization start (00:00). Black silhouettes at the embryo periphery are nuclei. Sqh-GFP (green) accumulates at furrow tips and then marks furrow ingression throughout cellularization. Gastrulation is evident after cellularization as apical relocalization of Sqh-GFP on the ventral side of the embryo (bottom of frame) and bending of the embryo surface.

Movie S2. Movie and analysis overlay showing the automated MATLAB code tracking furrow ingression; related to Figure 2. The code output is a plot of trajectories (right) showing position versus time. Sqh-GFP movie is the same as that shown in **Movie S1**. Regression of pseudocleavage furrows in mitotic cycle 13 precedes cellularization start (6 minutes). Colored circles, squares and triangles mark and track furrow tips. Gastrulation is evident after cellularization as bending of the embryo surface and splaying of trajectories (70 minutes).

Supplemental Experimental Procedures

Fly stocks

OreR was the wild-type stock for SEM and DIC. Stocks for live imaging were: Sqh-GFP (Royou et al., 2004), Gap43-mCherry (Martin et al., 2010), Spider-GFP (Morin et al., 2001), Venus-PH-PLCδ, and *shibire*^{ts}; Sqh-GFP (ts1 allele; Sweitzer and Hinshaw, 1998). For maternally induced RNAi, stock shRNA-*abl* (Bloomington #35327) was crossed with *mat67tub-GAL4* or *mat67tub-GAL4*; Sqh-GFP, and F1 mothers were crossed with sibling males. *abl* RNAi controls were *mat67tub-GAL4* or *mat67tub-GAL4*; Sqh-GFP.

Calculation of percent membrane stored in microvilli

To estimate the amount of membrane surface area contained in microvilli, we based our calculation on representative microvilli from an embryo in early cellularization (Figure S1A-1B). We considered two different shapes for these microvilli, based on the full range of microvillar morphologies that we observed from many embryos (n=42). For the first shape, the "finger model", each microvillus was considered as a top- and bottomless cylinder. Height and radius are in Table S1. The amount of membrane per microvillus was multiplied by the number of microvilli that can fit on the apical surface of each cell (61.6). Apical cell surface was considered as a dome (radius=2.6 μm; height=1.9 μm). The "finger model" represents a minimum value of microvillar surface area. For the second shape, the "hand model", microvilli were considered as a complex with a

wide base, or cylinder on its side (radius=1.5 μm; height=0.6 μm), with 5 microvilli atop the base, each as a top and bottomless cylinder (radius=0.3 μm; height=1.2 μm). The amount of membrane surface area per complex was multiplied by the number of "hands" containing 5 microvilli that could fit on each cell (12.3). The "hand model" represents a maximum value of microvillar surface area. To then calculate the amount of membrane required for furrow ingression, we calculated the final lateral surface area of a hexagonally shaped cell (radius=2.6 μm; height=36 μm). Finally, we divided the amount of membrane contained in microvilli by the amount of membrane required for furrow ingression. Error was calculated based on the standard deviation of measured microvillar dimensions. All dimensions were measured from SEM and multiplied by a scaling factor of 1.9 to account for shrinkage upon fixation. The average scaling factor was determined by comparing embryo measurements, including embryo diameter, final cell height and cell diameter, from SEM and live confocal images (1.9 ± 0.1; mean $\pm$ SD).

Calculation of endocytic events required for microvillar depletion

To estimate the number of endocytic events that would be required to consume the microvillar membrane, we assumed spherical vesicles with 100 nm diameter. From this, we calculated the rate of vesicle endocytosis that would be required to consume our estimated microvillar membrane surface area (averaged from minimum and maximum models; Figure 1C, Figure S1) according to the observed

ingression kinetics (Table S2). Endocytosis events were quantified as previously described (Sokac and Wieschaus, 2008).

Heat-shock for *shibire^{ts}*; Sqh-GFP

To assess ingression of 1x-WGA^{AX594} in *shibire^{ts}*; Sqh-GFP embryos, WGA was injected into the perivitelline space near the transition from slow to fast phase. Embryos were either held at permissive temperature (22°C) or in an incubator at restrictive temperature (32°C) for 10 minutes prior to imaging.

Venus-PH-PLCδ transgenesis and characterization

The PH domain of human Phospholipase Cδ1 (Met1-Ile175; Stauffer et al., 1998) was cloned into a modified pBluescript vector containing Venus and a multiple cloning site sandwiched between the 5' and 3' untranslated regions of *sqh*. The construct was inserted into pCasper4, and transgenesis done by BestGene, Inc. To confirm localization to microvilli, Venus-PH-PLCδ embryos were fixed in 8% formaldehyde/0.1 M sodium phosphate buffer (pH 7.4): heptane, and stained with anti-GFP antibody (1:500; Invitrogen A11120). Embryos were imaged on a Zeiss LSM 710 microscope with a 63X oil-immersion objective (NA=1.3).

Image processing and analysis

SEM images were analyzed in Photoshop (Adobe). Microvillar density was determined by averaging the number of microvillar tips in two 18 μm^2 boxes per

embryo from *en face* images, and progress through cellularization was scored by furrow length in cross-section. Since embryos shrink upon fixation, the ratio of furrow length to total embryo diameter was determined, and expressed as "normalized furrow length" for the density plot. Based on comparison to live embryos, the ingression velocity transition occurs at normalized furrow length=0.05.

For 4D data, z-stacks were collapsed in Zen (Zeiss) to give a maximum intensity projection (MIP) for each time point. Quantification of average intensity projections or summing voxels did not change the results. Embryos where cellularization extended past 75 minutes were suspected of phototoxicity (Figard and Sokac, 2011; Tinevez et al., 2012), and excluded from analysis. Per wild-type embryo (WT), intensities were normalized as $F_{norm}=(F-F_{min})/(F_{max}-F_{min})$. Normalized values per time point were averaged between embryos and plotted. The average fraction of signal depletion for "full" cellularization was calculated as $\Delta^{WT}=(F_{max}-F_{min})/F_{max}=0.50$ (n=4 buffer-injected Venus-PH-PLCδ embryos). For $slam^{RNAi}$, the average fluorescence intensity per MIP was calculated as for wild-type. To then relate $slam^{RNAi}$ data to wild-type, a theoretical value for F_{min} was first calculated per $slam^{RNAi}$ embryo as $F_{min}^{theor}=F_{maxslam}(1-\Delta^{WT})$, and was normalized as $F_{normslam}=(F_{slam}-F_{min}^{theor})/(F_{maxslam}-F_{min}^{theor})$. Normalized values per time point were averaged between embryos and plotted.

For measuring furrow ingression kinetics, a custom MATLAB (MathWorks) code was developed. The semi-automated code locates the edge of the embryo, creates a series of lines normal to the surface, and tracks the maximum fluorescence intensity (furrow tip) along each line as a function of time. Trajectories from 12 embryos were collapsed to a single start time at the beginning of cellularization, as set by the minimum furrow length for each trajectory. All ingression trajectories from a single embryo were averaged and then used to calculate average slow phase velocity, fast phase velocity, and timing and position of the velocity transition for all 12 embryos. Most embryos gave furrow trajectories that clustered when plotted (n=12), but embryos with velocities falling more than two standard deviations outside the mean (n=2) were excluded from analysis. Differential interference contrast (DIC) imaging of OreR wild-type embryos with no GFP probe reveals similar kinetics, confirming that Sqh-GFP does not induce ingression phenotypes (Table S2).

For *slam*^{RNAi} analysis, embryos were categorized as “no ingression” if 50 minutes after cellularization onset, furrow length still remained $\leq 6\ \mu$m.

For Sqh-GFP and WGA-injected embryos, kymographs were generated using custom MATLAB code.

Supplemental References

Figard, L., and Sokac, A.M. (2011). Imaging cell shape change in living *Drosophila* embryos. J Vis Exp. *49*, doi:10.3791/2503.

Knutton, S., Sumner, M.C.B., and Pasternak, C.A. (1975). Role of microvilli in surface changes of synchronized P815Y mastocytoma cells. J Cell Biol *66*, 568-576.

Martin, A.C., Gelbart, M., Fernandez-Gonzalez, R., Kaschube, M., and Wieschaus, E.F. (2010). Integration of contractile forces during tissue invagination. J Cell Biol *188*, 735-749.

Mooseker, M. and Tilney, L. (1975). Organization of an actin filament-membrane complex. J Cell Biol *67*, 725-743.

Morin, X., Daneman, R., Zavortink, M., and Chia, W. (2001). A protein trap strategy to detect GFP-tagged proteins expressed from their endogenous loci in *Drosophila*. Proc Natl Acad Sci USA *98*, 15050-15055.

Pelissier, A., Chauvin, J.P., and Lecuit, T. (2003). Trafficking through Rab11 endosomes is required for cellularization during *Drosophila* embryogenesis. Curr Biol *13*, 1848-1857.

Royou, A., Field, C., Sisson, J.C., Sullivan, W., and Karess, R. (2004). Reassessing the role and dynamics of nonmuscle myosin II during furrow formation in early *Drosophila* embryos. Mol Biol Cell *15*, 838-850.

Sokac, A.M., and Wieschaus, E. (2008). Local actin-dependent endocytosis is zygotically controlled to initiate *Drosophila* cellularization. Dev Cell *14*, 775-786.

Sweitzer, S.M., and Hinshaw, J.E. (2005). Dynamin undergoes GTP-dependent conformational change causing vesiculation. Cell *93*, 1021-1029.

Stauffer, T.P., Ahn, S., and Meyer, T. (1998). Receptor-induced transient reduction in plasma membrane PtdIns(4,5)P2 concentration monitored in living cells. Curr Biol *8*, 343-346.

Tinevez, J.Y., Dragavon, J., Baba-Aissa, L., Roux, P., Perret, E., Canivet, A., Galy, V., and Shorte, S. (2012). A quantitative method for measuring phototoxicity of a live cell imaging microscope. Methods Enzymol *506*, 291-309.